

Stable Half-Metallic Monolayers of FeCl_2

E. Torun,* H. Sahin, S. K. Singh,[†] and F. M. Peeters

Department of Physics, University of Antwerp, 2610, Antwerp, Belgium

(Dated: July 31, 2015)

The structural, electronic and magnetic properties of single layers of Iron Dichloride (FeCl_2) were calculated using first principles calculations. We found that the 1T phase of the single layer FeCl_2 is 0.17 eV/unit cell more favorable than its 1H phase. The structural stability is confirmed by phonon calculations. We found that 1T- FeCl_2 possess three Raman-active (130 , 179 and 237 cm^{-1}) and one Infrared-active (279 cm^{-1}) phonon branches. The electronic band dispersion of the 1T- FeCl_2 is calculated using both GGA-PBE and DFT-HSE06 functionals. Both functionals reveal that the 1T- FeCl_2 has a half-metallic ground state with a Curie temperature of 17 K.

PACS numbers: 81.05.ue, 85.12.de, 68.47.Fg, 68.43.Bc, 68.43.Fg

The synthesis of stable two-dimensional (2D) materials^{1,2} and observing their various exceptional physical properties triggered a large interest in their potential technological applications. Single layer transition-metal dichalcogenides (TMDs) are a new class of materials which are promising candidates for next generation of flexible nanoelectronic devices due to their wide range of important properties in their bulk and monolayer form such as superconductivity^{3,4} and half-metallicity.⁵⁻⁹

The single layer TMDs can be obtained from their three-dimensional (3D) counterpart which consist of weakly interacting 2D layered structures. Most of these materials have either D_{6f} (2H structure) or D_{3d} (1T structure) point-group symmetry and very few of them are stable in both the 1T and 2H phases. A lot of efforts are being done to predict new 2D materials theoretically and synthesize them experimentally with tailored electronic, optical, and chemical properties.

Half-metallicity is one of the desired properties for future spintronics devices and it is observed in 3D compounds several decades ago.¹⁰ Most of the 2D materials do not have intrinsic half-metallicity but it has been reported that graphene^{11,12} and hydrogenated boron-nitride nanoribbons¹³ gain half-metallicity when in-plane electric fields were applied. Chemical modification of the edges with different functional groups is also an alternative approach to achieve half-metallicity in 2D structures.^{14,15} It has been recently reported that graphitic carbon nitride ($\text{g-C}_4\text{N}_3$)^{16,17}, MnO_2 nanosheet with vacancies and monolayer chromium nitride¹⁸ show half-metallic behaviour.

FeCl_2 , which is a metal in its bulk form, is another member of family of TM crystals. Its bulk and molecular form have been investigated. Sarairoh and Altarawneh¹⁹ investigated the structure and thermodynamics stability of the FeCl_2 (100-Cl) surface using DFT calculations and found that the FeCl_2 (100-Cl) surface is the most stable configuration. The electronic energy levels and the Mössbauer spectroscopic parameters of FeCl_2 were calculated by Bominaar et al.²⁰ and by Mishra et al.²¹ at the self-consistent field level. The X-ray properties of FeCl_2 were reported by Chou et al.²² and Veal et al.²⁴ us-

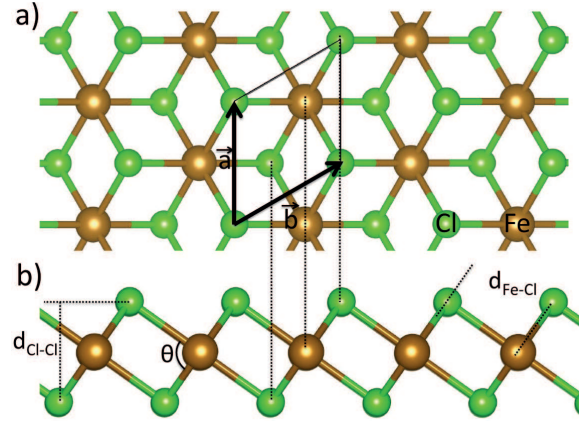


FIG. 1: (Color online) Atomic structure of 2D single-layer FeCl_2 in the T structure. (a) Top and (b) side views of the T structure showing the primitive unit cell of the 2D hexagonal lattice with Bravais lattice vectors \vec{a} and \vec{b} ($|\vec{a}|=|\vec{b}|$) and relevant internal structural parameters.

ing density functional theory. Shechter et al. performed a Mössbauer resonance study on FeCl_2 monolayers deposited on oriented basal planes of graphite.²³

In this work we will investigate the structural, electronic and vibrational properties of monolayer FeCl_2 by using first principle calculations. We will show that the minimum energy configuration of the single layer FeCl_2 is the T structure which has a half-metallic behaviour.

All the calculations are performed using the projector augmented wave (PAW)²⁵ potentials as implemented in the Vienna Ab-initio Simulation Package (VASP).^{26,27} The electronic exchange-correlation potential is treated within the spin polarized generalized gradient approximation (GGA) of Perdew-Burke-Ernzerhof (PBE).²⁸ A plane-wave basis set with kinetic energy cutoff of 500 eV is used. A vacuum spacing of more than 15 Å is taken to prevent layer-layer interactions. A set of $(20 \times 20 \times 1)$ Γ centered \mathbf{k} -point sampling is used for the primitive unit cell and scaled according to the sizes of the supercells used. The structures are relaxed until self-consistency is reached at the level of 10^{-5} eV between two consecutive steps and the atomic Hellman-Feynman force is less

than 10^{-4} eV/Å. Pressures on the lattice unit cell are decreased to values less than 1.0 kBar. For the charge transfer analysis, the effective charge on atoms is obtained by the Bader method.²⁹ More accurate electronic structure calculations were performed using the screened-nonlocal-exchange Heyd-Scuseria-Ernzerhof (HSE) functional of the generalized Kohn-Sham scheme.^{35,36}

Experimental and theoretical studies have shown that most of the compounds of transition metals form single layer crystal structures in T (TaS₂, VS₂, HfSe₂) or H (MoS₂, WSe₂, MoTe₂) phase. Our calculations show that the minimum energy configuration of a single layer FeCl₂ is the 1T structure. 1H structure of FeCl₂ is 0.17 eV/unit cell higher in energy than the 1T structure. In the 1T configuration, the Fe atoms are sandwiched between layers of trigonally arranged Cl atoms and each Fe atom is coordinated to six Cl atoms. The optimized atomic structure of hexagonal FeCl₂ lattice is shown in Fig. 1 and corresponding structural parameters are presented in Table I. The calculated lattice parameter, 3.47 Å, is in good agreement with previously reported experimental and theoretical values which are around 3.5 Å.^{19,30} However, the optimized lattice parameter of the H phase is 3.34 Å which is smaller than the one for the T phase. The Fe-Cl bond length is 2.45 Å in the T phase and is almost the same in the H phase which is 2.47 Å. Another possible phase of monolayer TMDs is the distorted T structure which was observed in ReS₂.³¹ In ReS₂, expanding the lattice parameter of the 1T-ReS₂ in one direction leads to a dimerization of Re atoms. This is responsible for an energetically more favorable distorted T structure. A similar investigation for the FeCl₂ monolayer revealed that the distorted T phase is not likely in this compound. This observation fits with earlier theoretical and experimental works.^{19,23,30,32}

The cohesive energy per unit cell of FeCl₂ is calculated by subtracting the total energies of the individual atoms from the total energy of FeCl₂ which is formulated as $E_c = E_T[Fe] + 2E_T[Cl] - E_T[FeCl_2]$. We found that the cohesive energy of FeCl₂ per unit cell is 2.64 eV/atom in the T phase which indicates a strong cohesion relative to the constituent free atoms and it is slightly higher than the value for the H structure which is 2.59 eV/atom.

TABLE I: Calculated values of stable, free-standing, 2D single-layer FeCl₂ in the T structure: lattice constant, $|\vec{a}|=|\vec{b}|$; bond lengths, d_{Fe-Cl} and d_{Cl-Cl} ; Cl-Fe-Cl bond angle, θ ; total magnetic moment per the unit cell, μ ; donated (received) electron by per Fe (Cl) atoms, ρ_{Fe} (ρ_{Cl}).

FeCl ₂ Phase	a (Å)	d_{Fe-Cl} (Å)	d_{Cl-Cl} (Å)	θ (deg)	μ (μ_B)	ρ_{Fe} (e)	ρ_{Cl} (e)	E_c eV/atom
1T	3.47	2.45	2.84	90.15	4	-1.20	0.60	2.64
1H	3.34	2.47	3.08	77.23	4	-0.86	0.43	2.59

FeCl₂ is not the only possible FeCl_n type structure in the monolayer form. Indeed, recently it was reported that FeCl₃ also exists.³³ In order to investigate the most

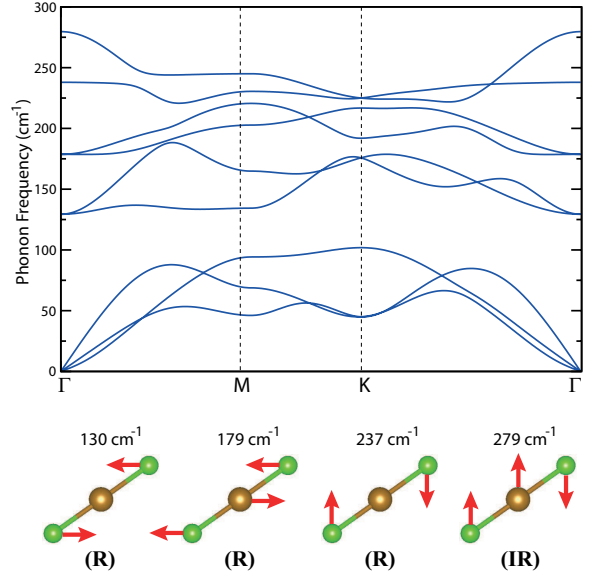


FIG. 2: (Color online) Phonon dispersion for the 1T phase of FeCl₂. Eigenfrequencies for Raman and Infrared-active modes and corresponding eigenmotions are shown in the lower panel.

favorable chemical composition of the compound, we calculated the cohesive energy of FeCl₃. The calculated cohesive energy of FeCl₃ is 2.4 eV/atom which is smaller than the value for the 1H and 1T phases of FeCl₂. This shows that the 1T phase of FeCl₂ is the most favorable monolayer structure of the FeCl_n type structures.

Phonon dispersion of the single layer FeCl₂ in the 1T phase is shown in Fig. 2. Here the dynamical matrix and the vibrational modes were calculated using the small-displacement method (SDM)³⁴ with forces obtained from VASP. We found that all the phonon branches have real eigenfrequencies through all the symmetry points and hence the predicted structure of 1T-FeCl₂ is dynamically stable.

There is one Fe atom and two Cl atoms within the primitive unit cell of 1T-FeCl₂ and its phonon spectrum includes 9 phonon bands, 3 acoustic (transverse acoustic TA, longitudinal acoustic LA, and out-of-plane transverse acoustic ZA) and 6 optical. While LA and TA acoustic branches have characteristics linear dispersion, the frequency of the out of plane ZA mode has a quadratic dispersion in the vicinity of the zone center. Analysis of the lattice dynamics shows that the decomposition of the vibration representation of optical modes (without translational acoustic modes) at the Γ point is $\Gamma_{opt} = 2E' + A_1' + 2E'' + A_2''$. We also show the optical character and frequency of the phonons for the monolayer FeCl₂ in the lower panel of Fig. 2. Note that while the phonon modes that have out-of-plane character (A_1' and A_2'') are singly degenerate, modes with in-plane vibrational character (E' and E'') are doubly degenerate.

In addition a large phonon energy bandgap, which is 130 cm⁻¹ at the Γ and 30 cm⁻¹ at the K point, is found between the acoustic phonon modes and the op-

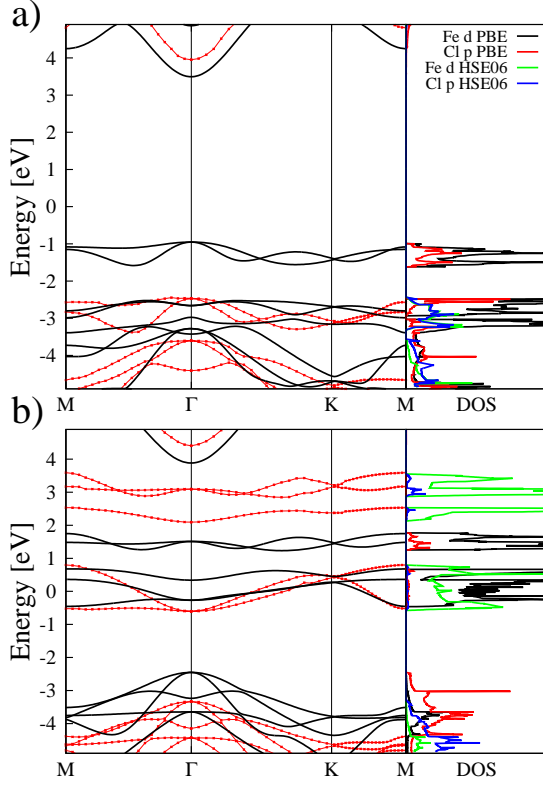


FIG. 3: (Color online) Electronic band structure of 2D single-layer FeCl_2 in the T structure and projected DOS of Fe and Cl atoms (a) minority and (b) majority states. The Fermi level of both calculations are set to 0 eV.

tical phonon modes. Due to the large phonon bandgap, the acoustic vibration is preserved from being interrupted by the optical modes and hence, FeCl_2 may have a higher quality factor than a graphene resonator.

FeCl_2 has a polar character in addition to the covalency of the bonds. Effective charge on cation and anion, Z_c^* and Z_a^* , charge transferred from cation to anion, $\delta\rho = Z_a^* - Z_v$ (Z_v being the valency of the constituent atom) are calculated using the Bader analysis. In spite of the ambiguities in finding the true effective charge, the calculated effective charges in Table I give some idea about the direction of charge transfer and ionicity of the honeycomb structure. Bader charge analysis showed that the Fe atom donates 1.20 e and each Cl atom receives 0.60 e charge in the T structure. In the H structure, however, Fe atom donates 0.86 e charge and each Cl atom receives 0.43 e charge.

In Fig. 3 the band structure and the density of states of FeCl_2 are shown for the minority (Fig. 3a) and the majority (Fig. 3b) states. The states which are around the Fermi level are mostly from the d-electrons of the Fe atom. The bands which are plotted in black in Fig. 3 are the results of PBE-GGA calculation. According to PBE-GGA calculations FeCl_2 show half-metallic property. An energy gap around 4.4 eV is observed in the electronic

structure of the minority states, however there are bands which are crossing the Fermi level in the case of the majority states which makes the compound a half metal. On top of PBE-GGA calculations we also performed HSE06 hybrid functional calculation to interpret the electronic structure of the compound more accurately. The HSE06 bands are shown in red in the band structure plots. As can be seen from the figure the half metallic behavior of FeCl_2 remains in the HSE06 calculations and the gap for the minority electrons increased to 6.7 eV.

Ferromagnetically ordered magnetic moments are a crucial requirement for spintronics devices. To find whether or not ferromagnetic state is energetically favorable, we perform supercell calculations and compare the energies of ferromagnetic and anti-ferromagnetic configurations. For FeCl_2 we compared the total energies of non-magnetic, ferromagnetic and anti-ferromagnetic configurations. The spin density plots of these calculations are shown in Fig. 4. Since the primitive cell of FeCl_2 has 4 μ_B magnetic moments, ferromagnetic configuration of 2×2 supercell (Fig. 4a) carries 16 μ_B . The anti-ferromagnetic configuration of 2×2 supercell (Fig. 4b) has 0 μ_B magnetic moment and 93 meV per primitive cell higher energy than the ferromagnetically ordered one. The non-magnetic configuration of FeCl_2 is 1.3 eV per primitive cell higher in energy than the ferromagnetic one. This means that the ferromagnetically ordered state is energetically the most favorable arrangement of FeCl_2 .

Curie temperature is defined as the temperature which separates the paramagnetic phase in which the magnetic moments are randomly oriented from the ordered ferromagnetic phase. The Curie temperature of the materials can be approximated using the Heisenberg model in which the Hamiltonian can be written as $\hat{H} = -\sum_{i,j} J \hat{m}_i \cdot \hat{m}_j$, where J is the Heisenberg exchange parameter and \hat{m} is the magnetic moment of each site in μ_B . The expression for the Heisenberg exchange parameter for our system is $J = (1/12)E_{ex}/2m^2$ where E_{ex} is the energy difference between ferromagnetic and anti-ferromagnetic configurations and the factor (1/12) is due to the double counting of the exchange interaction of 6 nearest neighbor atoms in the summation. If we substitute $m = 4$ and $E_{xc} = 372$ into the equation, we get $J = 0.97$ meV. There exist several approximations to find T_c from the J value. Here we will use the mean field approximation which is $k_B T_c = \frac{3}{2}J$. This approximation leads to a Curie temperature of 17 K. In addition, it is worthwhile to note that one may find different, but in the same order, T_c values using different methodologies^{18,37,38}.

To summarize, in this paper we investigated the structural, electronic and magnetic properties of single layers of FeCl_2 using first principles calculations. We found that the T phase is energetically more favorable than the H phase of the compound. Our vibrational analysis showed that all the phonon branches have real eigenvalues through all symmetry points which indicates the stability of the 1T- FeCl_2 structure. The electronic struc-

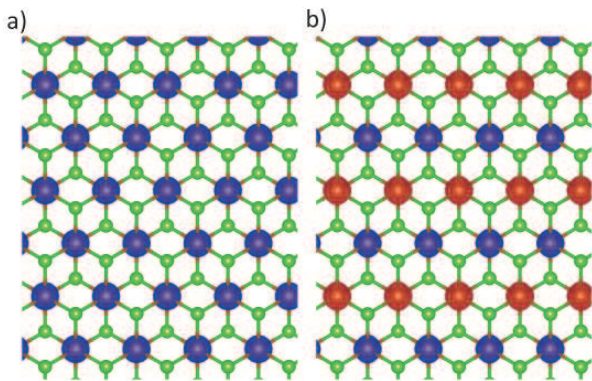


FIG. 4: (Color online) Spin density plot of (a) ferromagnetic and b) anti-ferromagnetic configurations of FeCl_2 . The blue lobes correspond to the minority and the red ones to the majority spin density.

ture of 1T-FeCl_2 is investigated using both GGA-PBE and DFT-HSE06 functionals. A very interesting physical property of the compound is revealed with both functionals: FeCl_2 has a half-metallic nature. Our supercell calculations showed that the ferromagnetic ordering of the magnetic moments have a lower energy than the anti-ferromagnetic ordered state. Thus, the 1T-FeCl_2 is an intrinsic half-metallic ferromagnet which makes it an attractive compound for future spintronics devices.

This work was supported by the Flemish Science Foundation (FWO-VI) and the Methusalem foundation of the Flemish government. Computational resources were provided by TUBITAK ULAKBIM, High Performance and Grid Computing Center (TR-Grid e-Infrastructure). H.S. is supported by a FWO Pegasus Long Marie Curie Fellowship.

* Electronic address: engin.torun@uantwerpen.be

† Current address: Department of Science and Technology, Linköping University, 60174 Norrköping, Sweden

- ¹ K. S. Novoselov, A. K. Geim, S. V. Morozov, D. Jiang, Y. Zhang, S. V. Dubonos, I. V. Grigorieva, A. A. Firsov, *Science* **306**, 666 (2004).
- ² S. Najmaei, Z. Liu, W. Zhou, X. Zou, G. Shi, S. Lei, B. I. Yakobson, J. -C. Idrobo, P. M. Ajayan, and J. Lou, *Nature Mater.* **12**, 754 (2013).
- ³ B. Sipos, A. F. Kusmartseva, A. Akrap, H. Berger, L. Farró, and E. Tutiš, *Nature Mater.* **7**, 960 (2008).
- ⁴ K. Takada, H. Sakurai, E. T.-Muromachi, F. Izumi, R. A. Dilanian, and T. Sasaki, *Nature (London)*, **422**, 53 (2003).
- ⁵ T. Shishidou, A. J. Freeman, and R. Asahi, *Phys. Rev. B* **64**, 180401 (2001).
- ⁶ Y. J. Jin and J. I. Lee, *Phys. Rev. B* **73**, 064405 (2006).
- ⁷ V. N. Antonov, O. V. Andryushchenko, A. P. Shpak, A. N. Yaresko, and O. Jepsen, *Phys. Rev. B* **78**, 094409 (2008).
- ⁸ S. Saha, M. De Raychaudhury, and T. S.-Dasgupta, *Phys. Rev. B* **77**, 155428 (2008).
- ⁹ M. O.-Leal, F. Rivadulla, M. García-Hernández, A. Piñeiro, V. Pardo, D. Baldomir, and J. Rivas, *Phys. Rev. B* **78**, 180415 (2008).
- ¹⁰ R. A. de Groot, F. M. Mueller, P. G. van Engen, and K. H. J. Buschow, *Phys. Rev. Lett.* **50**, 2024 (1983).
- ¹¹ Y. W. Son, M. L. Cohen, and S. G. Louie, *Nature (London)* **444**, 247 (2007).
- ¹² O. Hod, V. Barone, J. Peralta, and G. Scuseria, *Nano Lett.* **7**, 2295 (2007).
- ¹³ D. K. Samarakoon and X. Q. Wang, *Appl. Phys. Lett.* **100**, 103107 (2012).
- ¹⁴ T. B. Martins, A. J. R. da Silva, R. H. Miwa, and A. Fazzio, *Nano Lett.* **8**, 2293 (2008).
- ¹⁵ D. W. Boukhvalov and M. I. Katsnelson, *Nano Lett.* **8**, 4373 (2008).
- ¹⁶ A. Hashmi and J. Hong, *Sci. Rep.* **4** (2014).
- ¹⁷ T. Hu, A. Hashmi and J. Hong, *Sci. Rep.* **4**, 6059 (2014).
- ¹⁸ S. Zhang, Y. Li, T. Zhao, and Q. Wang, *Sci. Rep.* **4**, 5241 (2014).
- ¹⁹ S. A. Sarairoh and M. Altarawneh, *J. Chem. Phys.* **141**, 054709 (2014).
- ²⁰ E. L. Bominaar, J. Guillin, A. Sawaryn, and A. X. Trautwein, *Phys. Rev. B* **39**, 72 (1989).
- ²¹ K. C. Mishra, K. J. Duff, P. Kelires, S. K. Mishra, and T. P. Das, *Phys. Rev. B* **32**, 58 (1985).
- ²² S. H. Chou, F. W. Kutzler, D. E. Ellis, G. K. Shenoy, T. I. Morrison, and P. A. Montano, *Phys. Rev. B* **31**, 1069 (1985).
- ²³ H. Shechter, J. G. Dash, M. Mor, R. Ingalls, and S. Bukshpan, *Phys. Rev. B* **14**, 1876 (1976).
- ²⁴ B. W. Veal, D. E. Ellis, and D. J. Lam, *Phys. Rev. B* **32**, 5391 (1985).
- ²⁵ P. Blochl, *Phys. Rev. B* **50**, 17953 (1994).
- ²⁶ G. Kresse and J. Hafner, *Phys. Rev. B* **47**, 558 (1993).
- ²⁷ G. Kresse and J. Furthmüller, *Phys. Rev. B* **54**, 11169 (1996).
- ²⁸ J. P. Perdew, K. Burke, and M. Ernzerhof, *Phys. Rev. Lett.* **77**, 3865 (1996).
- ²⁹ G. Henkelman, A. Arnaldsson, and H. Jonsson, *Comput. Mater. Sci.* **36**, 354 (2006).
- ³⁰ C. Vettier and W. B. Yelon, *J. Phys. Chem. Solids* **36**, 401 (1975).
- ³¹ S. Tongay, H. Sahin, C. Ko, A. Luce, W. Fan, K. Liu, J. Zhou, Y.-S. Huang, C.-H. Ho, J. Yan, D. F. Ogletree, S. Aloni, J. Ji, S. Li, J. Li, F. M. Peeters, and J. Wu, *Nat Commun.* **5**, 3252 (2014).
- ³² M. K. Wilkinson, J. W. Cable, E. O. Wollan, and W. C. Koehler, *Phys. Rev.* **113**, 497 (1959).
- ³³ D. J. Wehenkel, T. H. Bointon, T. Booth, P. Bøggild, M. F. Craciun and S. Russo, *Sci. Rep.* **5**, 7609 (2014).
- ³⁴ D. Alfe, *Comp. Phys. Commun.* **180**, 2622 (2009).
- ³⁵ J. Heyd, G. Scuseria, and M. Ernzerhof, *J. Chem. Phys.* **118**, 8207 (2003).
- ³⁶ F. Fuchs, J. Furthmüller, F. Bechstedt, M. Shishkin, and G. Kresse, *Phys. Rev. B* **76**, 115109 (2007).
- ³⁷ J. Zhou and Q. Sun, *Journal of The American Chemical Society* **133**, 15113 (2011).
- ³⁸ H. Sims, S. J. Oset, W. H. Butler, J. M. MacLaren, and M. Marsman, *Phys. Rev. B* **81**, 224436 (2010).